Satellite Estimates of Wind Speed and Latent Heat Flux over the Global Oceans

ABDERRAHIM BENTAMY,* KRISTINA B. KATSAROS,+ ALBERTO M. MESTAS-NUÑEZ,#
WILLIAM M. DRENNAN,@ EVAN B. FORDE,+ AND HERVÉ ROQUET&

**Institut Français pour la Recherche et l'Exploitation de la Mer (IFREMER), Plouzane, France*
+NOAA/Atlantic Oceanographic and Meteorological Laboratory, Miami, Florida
#Cooperative Institute for Marine and Atmospheric Studies, University of Miami, Miami, Florida
@Rosenstiel School of Marine and Atmospheric Science, University of Miami, Miami, Florida
&Météo-France, Centre de Météorologie Spatiale, Lannion, France

(Manuscript received 3 September 2001, in final form 30 January 2002)

ABSTRACT

Surface fluxes of momentum, freshwater, and energy across the air–sea interface determine oceanic circulation and its variability at all timescales. The goal of this paper is to estimate and examine some ocean surface flux variables using satellite measurements. The remotely sensed data come from the European Remote Sensing (ERS) satellite scatterometer on *ERS-2*, NASA scatterometer (NSCAT), and several Defense Meteorological Satellite Program (DMSP) radiometers [Special Sensor Microwave Imager (SSM/I)] on board the satellites *F10–F14*. The sea surface temperature comes from daily analysis calculated from Advanced Very High Resolution Radiometer (AVHRR) measurements. This study focuses on the 9-month period (October 1996–June 1997) of the NSCAT mission. To ensure high quality of the merged surface parameter fields, comparisons between different satellite estimates for the same variable have been performed, and bias corrections have been applied so that they are compatible with each other. The satellite flux fields are compared to in situ observations from buoys and ships globally and in different regions of the ocean. It is found that the root-mean-square (rms) difference with weekly averaged wind speeds is less than 2.5 m s^{-1} and the correlation coefficient is higher than 0.8. For weekly latent heat flux, the rms difference between satellite and buoys does not exceed 30 W m^{-2}. The comparisons with weekly ship latent heat flux estimates gives an rms difference approaching 40 W m^{-2}. Comparisons are also made between satellite fields and atmospheric analyses from the European Centre for Medium-Range Weather Forecasts (ECMWF) and reanalyses from the National Centers for Environmental Prediction–National Center for Atmospheric Research (NCEP–NCAR). The wind speeds and latent heat fluxes from these atmospheric analyses compare reasonably well with the satellite estimates. The main discrepancies are found in regions and seasons of large air–sea temperature difference and high wind speed, such as the Gulf Stream during the winter season.

1. Introduction

Satellites have been demonstrated to measure ocean surface variables such as sea surface temperature (SST), sea surface height, surface wind, near-surface air humidity, and precipitation over the whole ocean at small spatial and short temporal scales. Several of these variables form the basis for estimations of the air–sea fluxes of momentum, freshwater, and heat. Satellite observations of ocean surface variables are, therefore, useful for climate analysis and forecasting (e.g., Grima et al. 1999), for investigating climatic variations in hurricane activity (Landsea et al. 1999; Goldenberg et al. 2001), and for monitoring the hydrologic cycle (e.g., op. cit., Schmitt and Wijffels 1993; Soden 1999). The complete sampling of the whole global ocean by polar-orbiting satellites is the compelling reason to use satellite observations for climatological studies and the motivation for this study. Here we examine details of the estimation of the latent heat flux (LHF) for a 9-month period and compare these estimates with in situ observations and atmospheric analyses.

The Wind Scatterometer instruments on the first and second European Remote Sensing satellite missions (*ERS-1* and *ERS-2*) have provided valuable observations of ocean surface winds since 1991. Taking advantage of consistent archives of these data covering almost a decade, a global database has been produced of gridded weekly and monthly wind vectors, bulk wind stress, wind divergence, and wind stress curl along with their corresponding error estimates (Bentamy et al. 1999). The ERS scatterometer data products are distributed to more than 1500 laboratories by the Centre ERS d'Archivage et de Traitement (CERSAT) through CD-ROMs or over the Internet. Within the ERS period, several flux-related

Corresponding author address: Dr. Kristina B. Katsaros, Office of Oceanic and Atmospheric Research, NOAA/Atlantic Oceanographic and Meteorological Laboratory, 4301 Rickenbacker Causeway, Miami, FL 33149.
E-mail: kristina.katsaros@noaa.gov

© 2003 American Meteorological Society

products have been estimated from the National Aeronautics and Space Administration (NASA) scatterometer (NSCAT) and Special Sensor Microwave Imager (SSM/I) [e.g., CERSAT Web site (http://www.ifremer.fr/cersat) and the Hamburg Ocean–Atmosphere Parameters from Satellite Data (HOAPS) Web site (http://www-pcmdi.llnl.gov/airseawg/catalogue/hoaps)].

Surface fluxes of momentum, freshwater, and heat provide some of the dominant processes responsible for climate variability. Direct observations of these fluxes over the global oceans are very demanding technologically and, consequently, rare. Hence, most estimates of the surface fluxes, whether from in situ or remote observations, or atmospheric analyses, rely on bulk formulas (e.g., Smith 1988; De Cosmo et al. 1996; Fairall et al. 1996) that parameterize the fluxes in terms of observed mean quantities. In the past, the various surface flux atlases (e.g., Bunker 1976; Esbensen and Kushnir 1981; Halpern et al. 1998; Isemer and Hasse 1987; da Silva et al. 1994; and many more) have used different versions of the bulk formulas and, as a result, the estimated fluxes vary significantly from one atlas to another. All bulk estimations of turbulent surface fluxes depend on surface wind measurements, whose importance for our study cannot be overly stressed. This fact is well illustrated by the evaluation of uncertainties in flux estimates by Gleckler and Weare (1997).

Knowledge of evaporation minus precipitation ($E - P$) over the ocean is essential for advancing the quantitative understanding of the global hydrologic cycle. About 78% of global precipitation and 86% of evaporation occurs over the oceans (Baumgartner and Reichel 1975). The value of $E - P$ controls the thermohaline circulation. Evaporation and, hence, latent heat flux, is thus an important variable for oceanographic studies. Jourdan et al. (1997) have performed satellite estimations of $E - P$ for the period 1988–90 and compared their results to model estimates and to the freshwater transport that can be inferred from oceanographic studies. These studies illustrate the need for satellite observations to improve our knowledge of this important and difficult aspect of ocean–atmosphere interactions.

In this paper, we present our methods for merging wind observations from several satellites and for estimating latent heat flux using wind fields, sea surface temperatures from daily global analysis calculated from the Advanced Very High Resolution Radiometer (AVHRR) measurements (Reynolds and Smith 1994), and near-surface atmospheric humidity observations from SSM/I. Using data from several satellites provides sufficient sampling to generate weekly wind fields and latent heat flux estimates. The resulting data are compared to collocated flux products from the two major numerical analysis centers, but the objective of this study is not verification of these models. We use the European Centre for Medium-Range Weather Forecasts (ECMWF) analysis and the National Centers for Environmental Prediction–National Center for Atmospheric Research (NCEP–NCAR) reanalysis. We also perform comparisons with in situ observations from ships and buoys, which we have considered closest to the ''truth,'' that is, the desired product, but only after thorough validation and corrections for known error sources.

The outline of the paper is as follows: in section 2, we present the datasets, along with the methods used to process the satellite data, as well as the weekly flux fields for the period October 1996–June 1997, when NSCAT was operational. This is followed by statistical comparisons of the satellite flux data to other flux estimates (section 3) and a discussion of the spatial and temporal variability present in these fields (section 4). Finally, in section 5 the main results are summarized and discussed.

2. Datasets and atmospheric analysis fields

Prior to describing the satellite data that are the focus of this work, we present brief descriptions of the in situ observations and the atmospheric model products that we use for comparison.

a. Buoys

Near-surface observations of wind speed and direction, air and sea surface temperatures and, on some platforms, relative humidity (or dewpoint), are provided by three buoy networks: the National Data Buoy Center (NDBC) buoys off the U.S. Atlantic, Pacific, and Gulf coasts maintained by the National Oceanic and Atmospheric Administration (NOAA; Fig. 1a); the European Offshore Data Acquisition System (ODAS) buoys in the eastern Atlantic, maintained by the U. K. Met Office (UKMO) and Météo-France (Fig. 1b); and the Tropical Atmosphere Ocean (TAO) buoys located in the tropical Pacific Ocean and maintained by NOAA's Pacific Marine Environmental Laboratory (PMEL; Fig. 1c). Atmospheric measurements are made at a height of about 4 m. For comparison with remotely sensed winds and latent heat fluxes, the Liu–Katsaros–Businger (LKB) model (Liu et al. 1979) is used to calculate 10-m wind speeds and humidities (when measured) at neutral conditions.

b. Ships

Our remotely sensed wind and latent heat flux estimates are also compared to the Comprehensive Ocean–Atmosphere Data Set (COADS). COADS is mostly based on quality-controlled marine surface observations from ships, but they have been supplemented in more recent years with moored environmental buoys, drifting buoys, and near-surface measurements from oceanographic profiles. The COADS observational records and metadata used in this study come from the latest available version of the COADS dataset that will be part of release 2 (Woodruff et al. 1998).

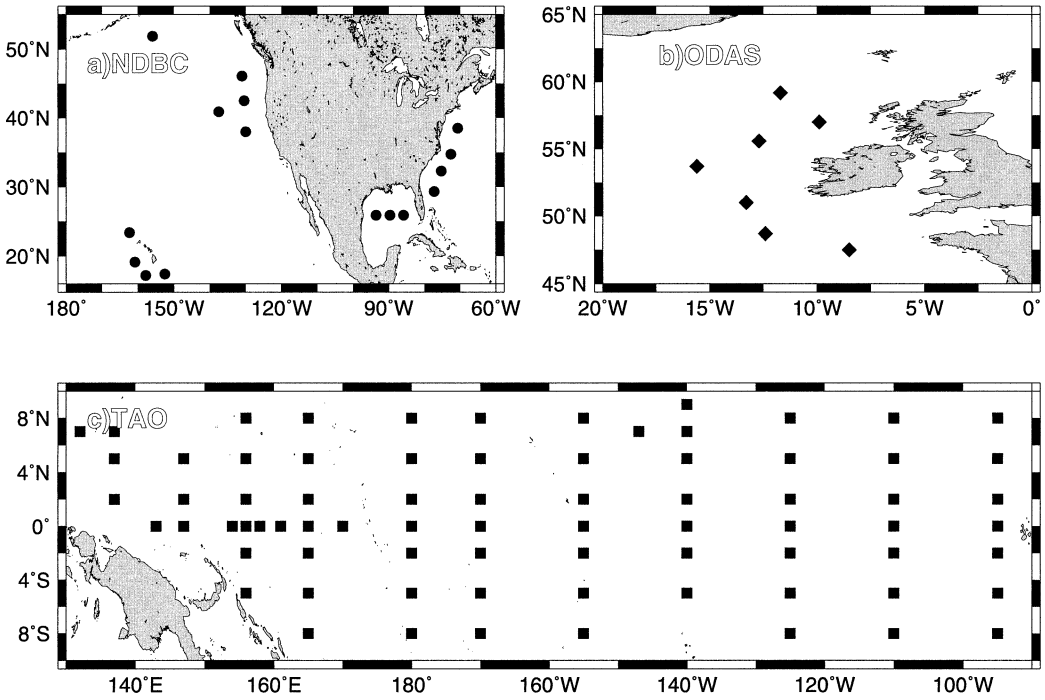

FIG. 1. Locations of the (a) NDBC, (b) ODAS, and (c) TAO buoy networks used in this study.

Only those COADS data records with valid measurements of wind speed, air temperature, SST, dewpoint, and position are used in this study. The data were further quality controlled to remove outliers, using limits based on comparing all available data in given temporal and spatial windows. In a few cases, entire ship tracks were removed due to evident instrumental biases. Corrections were applied to individual records as follows: SST values measured with ship intake thermometers were reduced by 0.35°C (Kent and Taylor 1995); wind speeds reported using the Beaufort scale [World Meteorological Organization (WMO) 1100 standard] were adjusted using the revised Beaufort scale of Lindau (1995; see also da Silva et al. 1995); data were adjusted to 10-m neutral values assuming logarithmic profiles and sensor heights of 15 m, consistent with the median anemometer height reported by Taylor et al. (1995). Weekly averages of individual 10-m neutral records were then made based on a $2° \times 2°$ grid. This forms the basis for the COADS dataset used here.

The COADS data were further validated by comparison with data from ODAS buoy 62029 located at 48.7°N, 12.4°W. For the comparison, all validated ship data collected within a $1° \times 1°$ box centered on the buoy during the 15-month period July 1996–September 1997 were used. The buoy data, measured at 4 m, were transformed to 10-m neutral values following the same procedure as for the ship data. The 267 ship data points were compared with ODAS data interpolated from the hourly time series. The correlation coefficients for U, SST, T_a, and T_{dew} comparisons were 0.77, 0.86, 0.89, and 0.86, respectively. For the three temperatures, no significant differences between ODAS and ship data were found [differences were on the order of $0.5° \pm 2°$C (one standard deviation)]. For wind speed, the ODAS winds appear to be biased low by about 1.1 m s^{-1}, confirming the earlier comparisons of ODAS with model and satellite results (Bentamy et al. 2002).

c. Atmospheric analyses

In this study, we use ECMWF atmospheric analyses and NCEP–NCAR atmospheric reanalysis fields. The ECMWF fields are 10-m wind vectors and surface latent heat fluxes, provided by Météo-France through the Archivage, Validation, et Interprétation des données des Satellites Oceanographiques (AVISO) database. In 1996–97, the numerical weather prediction (NWP) system operational at ECMWF was relying on a global atmospheric spectral model, with a T213 truncation, and a three-dimensional variational incremental assimilation system, based on the computation of increments at a T63 truncation (Courtier et al. 1998). In 1996–97, the assimilated observations included mainly in situ observations from the global tracking system (GTS), cloud-track winds from geostationary satellites, the Television Infrared Observation Satellite (TIROS) Operational Vertical Sounder (TOVS) radiances from NOAA polar-orbiting satellites, and scatterometer winds from *ERS-2*.

The ECMWF analysis fields were interpolated to a regular $1° \times 1°$ grid. The 10-m wind vectors were pro-

TABLE 1. Weeks used for the comparison of satellite-derived weekly fields with ECMWF and NCEP–NCAR atmospheric analyses.

Week	Dates
1	30 Sep–6 Oct 1996
2	7–13 Oct 1996
3	14–20 Oct 1996
4	21–27 Oct 1996
5	28 Oct–3 Nov 1996
6	6–12 Jan 1997
7	13–19 Jan 1997
8	20–26 Jan 1997
9	27 Jan–2 Feb 1997
10	7–13 Apr 1997
11	14–20 Apr 1997
12	21–27 Apr 1997
13	28 Apr–4 May 1997
14	2–8 Jun 1997
15	9–15 Jun 1997
16	16–22 Jun 1997
17	23–29 Jun 1997

duced by the 3DVAR analysis every 6 h, and the surface latent heat fluxes are integrated values over 6 h, produced by the model during the first 6 h of the forecast after the analysis. As a boundary condition over the ocean, the ECMWF weather prediction system uses the SST analysis, produced and distributed daily by NOAA/NCEP (Reynolds and Smith 1994). In the model, turbulent surface fluxes are parameterized with bulk aerodynamical formulas, with turbulent transfer coefficients depending on wind speed and atmospheric stability (Louis 1979).

The NCEP–NCAR atmospheric reanalysis fields were obtained from the NOAA Climate Diagnostic Center Web site. For a detailed description of how these reanalysis fields are generated, see Kalnay et al. (1996). We used the NCEP–NCAR 4 times daily surface wind speed fields (which we constructed from the 10-m wind vector fields) and daily averaged latent heat fluxes, both available on a global Gaussian grid at $2^\circ \times 2^\circ$.

For comparison with the satellite observations, we constructed weekly averaged ECMWF and NCEP–NCAR wind speed and latent heat flux fields. The available ECMWF 6-hourly analyses allowed calculating weekly averaged fields for 17 weeks (Table 1) in our period of interest (October 1996–June 1997). For consistency, the comparison between satellite and NCEP–NCAR weekly fields is also limited to these 17 weeks.

d. Satellite wind speed

During the period October 1996–June 1997, two satellite scatterometers and four satellite radiometers supplied abundant surface observations over the global oceans.

One scatterometer was onboard *ERS-2* and measured the backscatter return from the sea surface of a 5.3-GHz electromagnetic signal emitted at various incidence angles. The other scatterometer was NSCAT, onboard the first *Advanced Earth Observation Satellite* (*ADEOS-1*), which used a 14.1-GHz signal. The backscatter energy is proportional to the spectral energy density of the Bragg backscattering waves, which have wavelengths on the order of centimeters. The energy received from the small ripple waves is mainly related to the surface wind, that is, to the wind stress (Bentamy et al. 1994; Quilfen 1995; Jet Propulsion Laboratory 1996).

The SSM/I radiometers onboard the Defense Meteorological Satellite Program (DMSP) *F10*, *F11*, *F13*, and *F14* satellites provide measurements of the surface brightness temperatures at frequencies of 19.35, 22.235, 37, and 85 GHz (hereafter referred to as 19, 22, 37, and 85 GHz), respectively. Horizontal and vertical polarization measurements are taken at 19, 37, and 85 GHz, but only vertical polarization is available at 22 GHz. Due to the choice of the channels operating at frequencies outside strong absorption lines (for water vapor; 50–70 GHz), the radiation observed by the antennae is a mixture of radiation emitted by clouds, water vapor in the air and the sea surface, as well as radiation emitted by the atmosphere and reflected at the sea surface. Several semiempirical models exist that relate SSM/I brightness temperature measurements to the total integrated water vapor (W), total integrated liquid water (L), surface wind speed at 10-m height and neutral stratification (U_{10N}), and bottom layer integrated water vapor (W_B; e.g., Goodberlet et al. 1989; Petty and Katsaros 1994; Wentz et al. 1986; Schulz et al. 1993; Schlüssel et al. 1995; Schulz et al. 1997). We further discuss the models for water vapor content in the next section.

The raw scatterometer and radiometer data are retrieved from the CERSAT database. The 10-m wind speed and direction derived from scatterometer measurements are provided along one swath 500 km wide for the *ERS-2* scatterometer, and two swaths 600 km wide for NSCAT. The spatial resolution of the scatterometer wind vector observations is 50 km $\times$ 50 km. The *ERS-2* wind vectors used in this study are estimated from *ERS-2* backscatter coefficients based on the CERSAT wind algorithm (Maroni 1996) and on a new formulation of the geophysical model function (CMOD-I2). The latter includes a bias correction for *ERS-2* wind estimates (Bentamy et al. 2002). The NSCAT winds come from the Jet Propulsion Laboratory (JPL) (Jet Propulsion Laboratory 1996). For estimation of the 10-m wind speed from SSM/I brightness temperatures, we use an algorithm published by Bentamy et al. (1999). This algorithm is a slightly modified version of that published by Goodberlet et al. (1989) that includes a water vapor content correction. The SSM/I wind speeds are calculated over swaths of 1394-km width, with a spatial resolution of 25 km $\times$ 25 km. The accuracies of the scatterometer and SSM/I winds during the NSCAT period (October 1996–June 1997) are evaluated by a comparison with wind speed and direction measured by moored buoys (Bentamy et al. 2002). The standard error of *ERS-2*, NSCAT, and SSM/I wind speeds with respect to the

buoy winds are about 1.35, 1.30, and 1.70 m s^{-1}, respectively. The bias values do not exceed 0.20 m s^{-1} (except for ODAS, as discussed in section 2b).

Our approach is to maximize global coverage by merging all satellite wind fields into a single weekly gridded wind field. By increasing the number of samples, the mean-square error is reduced. The general consistency between the three remotely sensed wind observations is investigated through linear statistical comparisons. Each instrument is collocated with the others within space and time windows of 50 km and 1 h, respectively. For instance, the maximum value of the bias between the global satellite wind speeds does not exceed 0.20 m s^{-1} (obtained for $U_{\mathrm{ERS2}} - U_{\mathrm{F10}}$). The standard deviation of the wind speed differences over the global oceans $\sigma(U_{\mathrm{ERS2}} - U_{\mathrm{F10}})$, $\sigma(U_{\mathrm{ERS2}} - U_{\mathrm{NSCAT}})$, and $\sigma(U_{\mathrm{NSCAT}} - U_{\mathrm{F10}})$, are 2.01, 1.90, and 1.14 m s^{-1}, respectively. The smallest correlation coefficient value that is obtained for the $U_{\mathrm{ERS2}}/U_{\mathrm{F10}}$ comparison is 0.84 (Bentamy et al. 1999).

e. Satellite latent heat flux

1) METHODS FOR EVAPORATION CALCULATION

The latent heat flux is generally described by

$$Q_E = l\rho\overline{w'q_a'}, \tag{1}$$

where Q_E is the latent heat flux, l is the latent heat of evaporation, ρ is the air density, w is the vertical component of velocity, and q_a is the near-surface air specific humidity. The horizontal bar indicates time averaging and the primes turbulent fluctuations from this temporal mean. Since Eq. (1) is difficult to evaluate, the latent heat flux is usually estimated using the following bulk aerodynamic parameterization, which is suitable for both satellite and in situ surface observations:

$$Q_E = -l\rho C_E(\overline{U}_a - \overline{U}_s)(\overline{q_a} - \overline{q_s}), \tag{2}$$

where C_E is the bulk transfer coefficient for water vapor (also called the Dalton number), U_a is the surface wind speed at a height of typically 10 m, U_s is the ocean surface speed (or surface current) usually set to 0, and q_s is the air specific humidity just above the air–sea interface.

The calculation of Q_E using Eq. (2) implies knowledge of three key variables:

1) Surface wind speed at 10-m height (U_a, hereafter U_{10}): U_{10} is derived from *ERS-2*, NSCAT, and SSM/I observations, as indicated in the previous section, for neutral atmospheric stratification.
2) SST (hereafter also indicated by T_s): The humidity just above the air–sea interface, q_s, is calculated from T_s assuming saturation at the surface. This q_s is reduced by 2% to account for salinity effects (the same correction is applied to the in situ data). Here T_s is derived from the AVHRR on board NOAA satellites. This variable can be obtained from several sources: the Physical Oceanographic Data Active Archive Center (PODAAC) of JPL; daily optimally interpolated (OI) SST data calculated by the Reynolds and Smith (1994) method at NCEP. For this study, the SST analysis for AVHRR data has been provided by AVISO/Météo-France based on the global, daily Reynolds OI product on a $1^\circ \times 1^\circ$ grid.
3) Surface layer air specific humidity (q_a): Several authors have investigated the estimation of q_a from microwave radiometer measurements. For instance, Liu (1986), using a large database containing 17 yr of soundings from ship and ocean-island stations, showed that q_a (not necessarily at a 10-m height) is well correlated with the integrated water vapor content, W. The latter can be derived from SSM/I brightness temperatures. This method provides accurate values of global monthly averaged q_a but exhibits a systematic bias of over 2 g kg^{-1} in the Tropics, as well as in the mid- and high latitudes (Esbensen et al. 1993). To reduce this bias, Miller and Katsaros (1992) derived regressions of the air–sea humidity difference as a function of W. Their model improved the estimation of instantaneous values, but it is limited to the northwest Atlantic. Schulz et al. (1993) provided a model to estimate the SSM/I precipitable water of the lowest 500-m layer of the planetary boundary layer (bottom-layer-integrated water vapor W_B instead of W). The calibration of the SSM/I W_B is based on 542 globally distributed soundings derived from meteorological field experiments. In addition, they derived a linear relationship between W_B and q_a. Ataktürk and Katsaros (1998) applied the Schulz et al. (1993) model to individual estimations and found that it overestimated q_a values in the subtropics. Schlüssel et al. (1995), using a larger dataset of soundings, determined a new version of the Schulz model. In this model, q_a is derived directly from SSM/I brightness temperature measurements.

Several of the inverse models relating the specific humidity of air and SSM/I brightness temperature measurements were investigated through comparison with observations of q_a from ships. The model described by Schulz et al. (1993, 1997) provides better agreement with in situ q_a estimates than previous models. However, our comparisons indicated seasonal and regional biases between ship q_a and satellite q_a calculated using the Schulz model (Fig. 2). For instance, in the North Atlantic, this bias was about -0.22 g kg^{-1} during the summer season, while in winter and spring seasons it increased to about 0.7–0.8 g kg^{-1}. Comparisons between ship and ODAS buoy q_a estimates did not show such biases (not shown). Therefore, to minimize these biases between satellite and in situ air specific humidity, a sample of 1000 pairs of collocated SSM/I brightness temperatures and ship data was used to estimate new values for the coefficients in the Schulz model. The collocation is performed over the global oceans, using

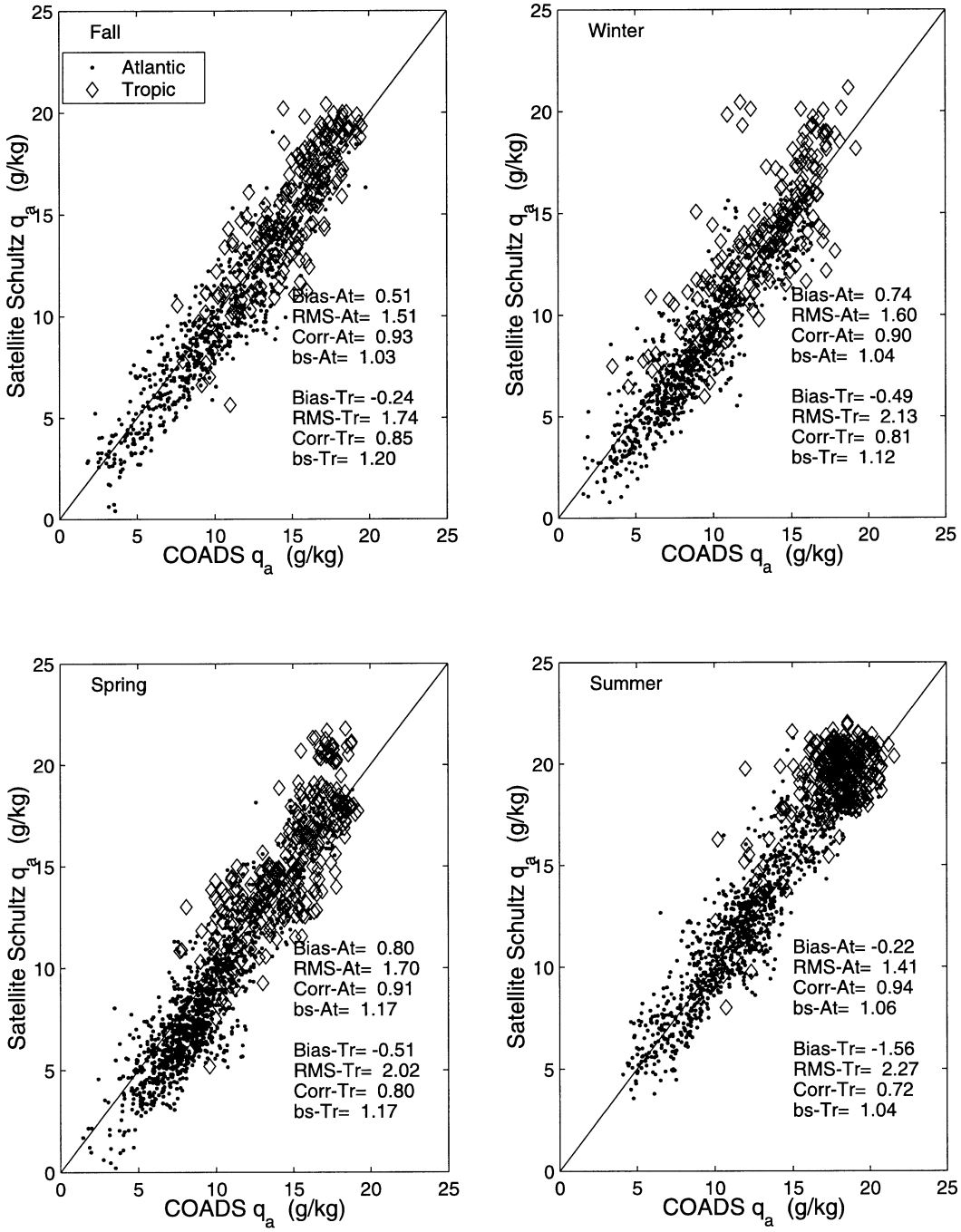

FIG. 2. Comparisons between specific air humidity estimated from ship (COADS) measurements and from merged satellite observations during fall, winter, spring, and summer seasons from Oct 1996 to Sep 1997.

all available and validated satellite (*F10*, *F11*, *F13*, and *F14*) and ship data during the period October 1996–September 1997. The collocated ship q_a data are divided into bins of 0.5 g kg^{-1}. From each q_a class, 20 of the collocated ship/satellite data were randomly selected. The q_a model coefficients were determined by minimizing the squared differences between observed q_a (from ship) and estimated q_a (from satellite). The new model and its coefficients are provided by the following equation:

$$q_a = a_0 + a_1 T_{19V} + a_2 T_{19H} + a_3 T_{22V} + a_4 T_{37V}, \quad (3)$$

where $a_0 = -55.9227$, $a_1 = 0.4035$, $a_2 = -0.2944$, $a_3 = 0.3511$, and $a_4 = -0.2395$.

The remaining collocated ship/satellite data are used to compare in situ and remotely sensed q_a estimates. As

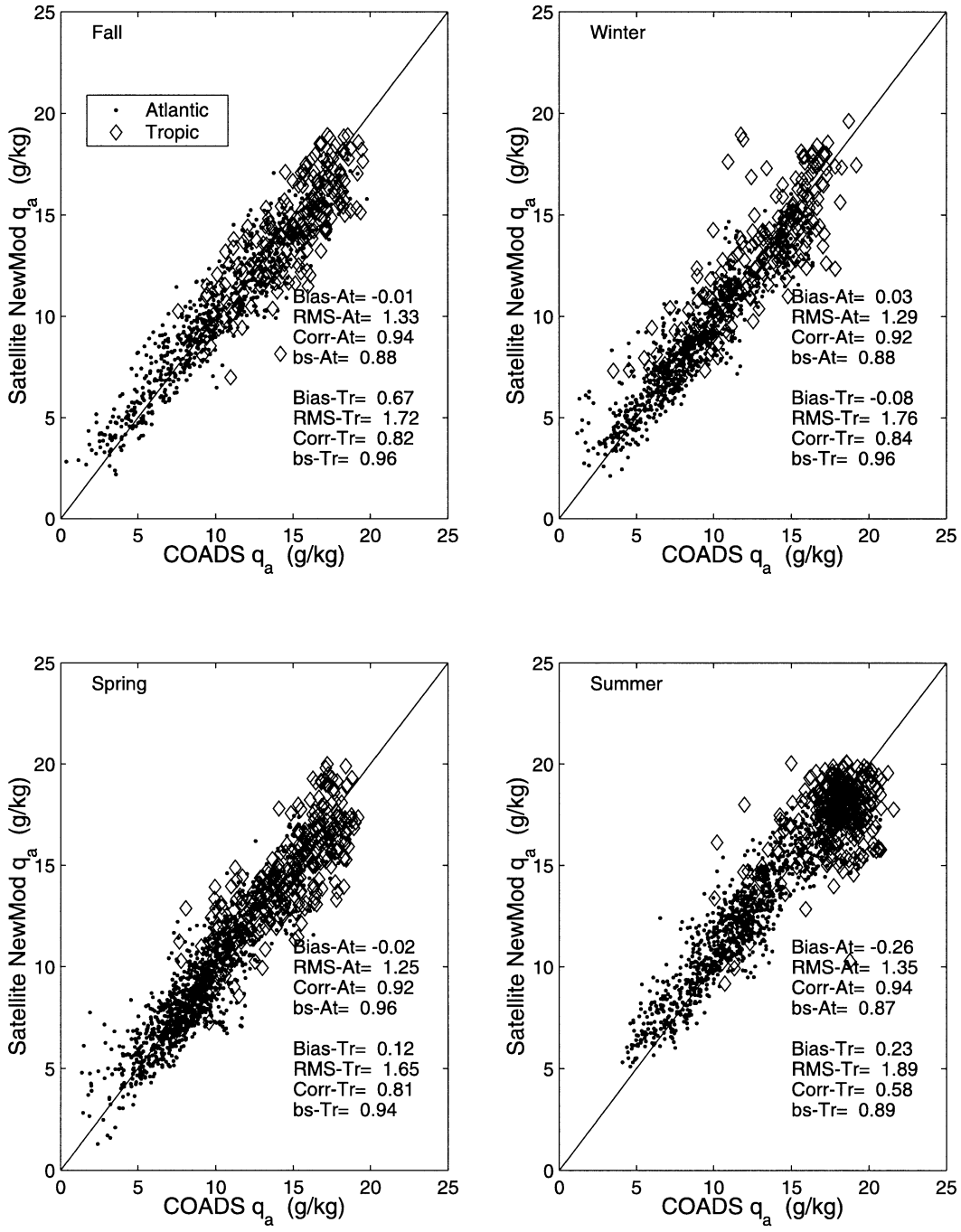

FIG. 3. Similar to Fig. 2, except satellite air humidity is calculated from the model given by Eq. (3).

expected, the comparisons of the statistical parameters are improved using the new q_a model (Fig. 3). On average, the bias is reduced by 15% and is no longer statistically significant. The rms difference between satellite and ship q_a estimates is now 1.40 instead of 1.70 g kg^{-1}. Over the North Atlantic Ocean (80% of ship data are located in this region), the maximum values of the difference bias between satellite and ship q_a is about 0.25 g kg^{-1} and is found during the summer season, where q_a values are high.

Based on the behavior of C_E as a function of wind speed and air–sea temperature difference (Smith 1988) and assuming slightly unstable stratification over the global ocean ($T_s - T_a = 1.25$°C), along with the Hasse and Smith (1997) results for the neutral C_E, the Dalton number is computed using the following fit:

$$10^3 C_E = a \exp[b(U_{10} + c)] + \frac{d}{U_{10}} + 1, \quad (4)$$

where $a = -0.146\,785$, $b = -0.292\,400$, $c = -2.206\,648$, and $d = 1.611\,229\,2$. The C_E values range between 0.0015 and 0.0011 for wind speeds between 2 and 20 m s^{-1}. For completeness, our expressions for latent heat of evaporation, air density, and saturated surface humidity are, respectively,

$$l = 4186.8(597.31 - 0.5625T_s), \quad (5)$$

$$\rho = \frac{100P_0}{287T_v}, \quad (6)$$

$$q_s = \frac{0.622e_s}{P_s - e_s}, \quad (7)$$

where $T_v = T_{10}\,(1 + 0.608\,q_a)$, and $e_s = T_s^a \times 10^{(b+c/T_s)}$, $a = -4.928$, $b = 23.55$, and $c = -2937$. These latter coefficients include the 2% reduction of surface humidity due to salinity effects. In these equations, wind speed, temperature, and pressure are in m s^{-1}, K, and hPa, respectively.

2) Error analysis

Using Eq. (2) to estimate individual latent heat flux values implies that there is an inherent Q_E error mainly related to the errors on each input parameter (e.g., Gleckler and Weare 1997). A simple simulation of the rms error is presented below to illustrate this issue. Let us consider variables U, T_s, and T_a, ''ground truth'' for wind speed, SST, and air temperature as retrieved from global ship data during October 1996–June 1997. The Dalton number, C_E, the specific surface humidity, q_s, and the latent heat flux, Q_E, are calculated from U, T_s, q_a, and T_a. To explain the structure of the Q_E bias, we calculate $\tilde{Q}_E$, from Eq. (2), which is the biased Q_E due to a bias on wind speed ($\tilde{U} = U + \varepsilon_u$), on surface temperature ($\tilde{T}_s = T_s + \varepsilon_{T_s}$), on exchange coefficient ($\tilde{C}_E = C_E + \varepsilon_{CE}$), or on specific humidity of the air ($\tilde{q}_a = q_a + \varepsilon_{q_a}$). For instance, the $\tilde{Q}_E$ bias due to a U bias of 1 m s^{-1} is 10 W m^{-2} for T_s less than 10°C. In tropical areas where T_s is above 22°C, the impact of the U bias on Q_E accuracy is large, and the consequent Q_E bias exceeds 20 W m^{-2}. The Q_E bias due to a 10% error in C_E exceeds 10 W m^{-2} for U and T_s higher than 7 m s^{-1} and 20°C, respectively. The sensitivities of Q_E to the errors in T_s and q_a are also quite large. The Q_E bias due to a 1°C bias in T_s typically exceeds 10 W m^{-2} for U greater than 7 m s^{-1} and T_s greater than 10°C. The Q_E bias due to a 1 g kg^{-1} bias in q_a exceeds 20 W m^{-2} for U greater than 7 m s^{-1}.

The error in wind speed, exchange coefficient, SST, and specific air humidity used in our satellite latent heat fluxes can be related to various sources: instrumental errors, calibration/validation of inverse models relating satellite measurements to geophysical parameters, boundary layer models, sampling schemes, and aliasing problems. The accuracy of surface winds derived from satellite data is discussed in section 2c. The main published C_E models are comparable within 5 and 12 m s^{-1}. The larger differences are located in the low (<3) and high (>16 m s^{-1}) wind speed ranges. The comparisons (not shown) between all available and validated daily average in situ (buoys and ships) SSTs and the Reynolds daily SST analysis indicate that the SST bias does not exceed 0.1°C, and that there are no significant seasonal or regional difference features.

3) Calculation of evaporation

Before using Eq. (2), which requires the knowledge at each grid point and at a given time of T_s, U_{10}, and brightness temperatures for the individual calculation of Q_E, some quality control and calculations are done over each satellite swath and sensor cell. Indeed, merging radar and radiometer data implies a strict quality control on the satellite observations. In addition to the quality flags (including land and ice masks) provided within each satellite product, we impose the following conditions:

1) For scatterometers (*ERS-2*, NSCAT): All scatterometer data with a high maximum likelihood estimator (difference between measured and estimated backscatter coefficients) are excluded.
2) For SSM/I: Any cell where rain is present or the liquid water vapor content is higher than 40 kg m^{-2} (Bentamy et al. 1999) is excluded. The latter parameters are both estimated from SSM/I brightness temperatures (Petty and Katsaros 1992). The same masks used to delete pixels over land or ice for *ERS-2* processing are also used for SSM/I.

The calculation of Q_E is performed hourly, with a spatial resolution of 1° in latitude and 1° in longitude. This resolution is consistent with that of the Reynolds daily gridded maps used for SST retrieval. Prior to calculating Q_E, all available data (winds, SSTs, and brightness temperatures), sampled within a 1° × 1° grid point of a satellite swath during a given hour, are averaged, and the two first statistical moments are computed. Figure 4 shows an example of satellite-validated wind observations as a function of time at three grid points during a 3-day period. As expected, the number of satellite observations in high latitudes is larger than in mid- or tropical latitudes. Figure 4 also indicates that at high latitudes, one can expect one scatterometer and one radiometer data sample in a 6-h window with about a 50% chance.

Over each grid point located within each SSM/I swath, the available U_{10}, T_s, T_{19V}, T_{19H}, T_{22V}, and T_{37V} are used to estimate the instantaneous latent heat flux values through Eqs. (2)–(7). In case the SSM/I wind speeds are not valid, scatterometer winds (*ERS-2*, NSCAT) calculated over the same grid point and within a 3-h window

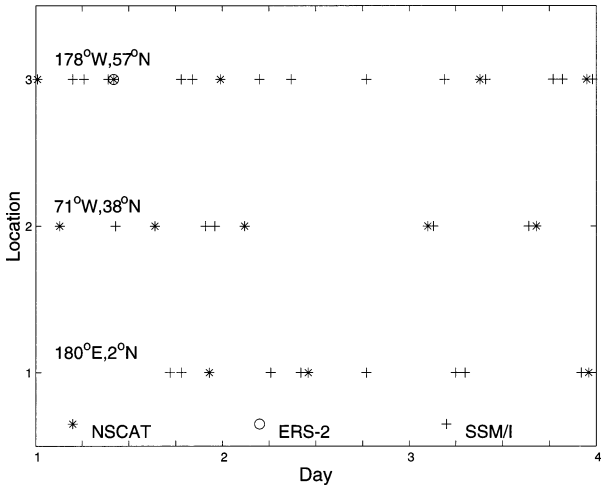

FIG. 4. Example of the occurrence of satellite wind observations as a function of time at three grid points and during a 3-day period.

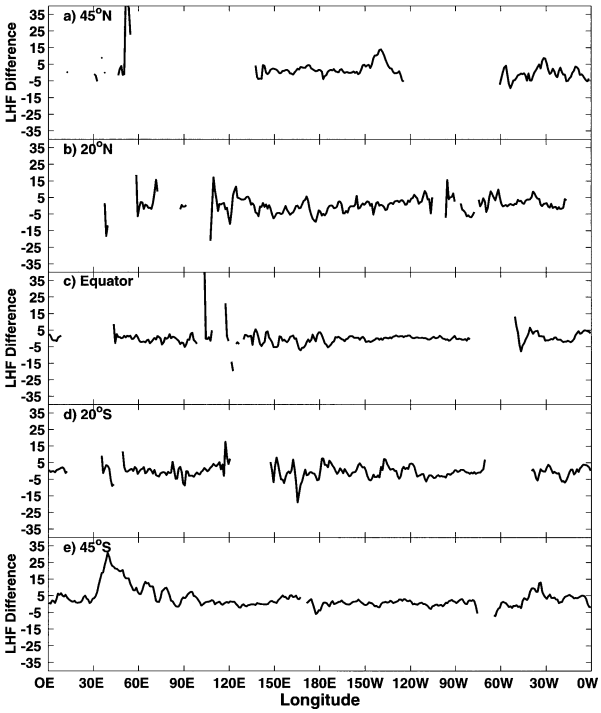

FIG. 5. Behavior of the difference between weekly gridded latent heat fluxes, calculated from 6-h ECMWF analysis and from simulated merged satellite data, as a function of longitude at five latitudes: (a) 45°N, (b) 20°N, (c) equator, (d) 20°S, and (e) 45°S.

are temporally interpolated to the time of the SSM/I observations. On average, the percentage of individual latent heat fluxes estimated with scatterometer wind speeds is about 15% for NSCAT and 9% for *ERS-2*. This number increases in tropical areas (10°S–10°N) to 19% for NSCAT and to 12% for *ERS-2*.

Several assumptions have been made for the calculations described above. The SST at a grid point is assumed constant over a day. The surface pressure P_0 is assumed to be at a constant value of 1013.25 hPa. Air temperature at 10 m, T_{10}, is taken to be $T_s - 1.25$ K. The impact of these assumptions on bulk latent heat flux estimation has been investigated with buoy measurements, which provide surface pressure, air temperature, and sea surface temperatures. The possible error (uncertainty) due to these assumptions is generally less than 2.5%.

f. Weekly wind speed and latent heat flux

The objective analysis of satellite wind and latent heat flux observations is based on the kriging method described by Bentamy et al. (1996). The method is applied to surface winds and latent heat flux fields separately. The aim is to calculate global weekly averaged flux parameters on a grid of 1° × 1° resolution. The interpolation scheme uses a spatial and temporal structure function describing the variable's behavior. The algorithm provided by Bentamy et al. (2002) is used to calculate gridded wind fields. The structure function for latent heat flux is determined, and the spatial and temporal correlation scales calculated from satellite observations are about 1510 km and 65 h, respectively. These parameters are then used to evaluate the weights of the satellite observations required to estimate the weekly value, depending on their spatial and temporal position relative to the grid point under analysis. As can be expected, the number of these observations is a function of latitude (Fig. 4). On average, more than 336 observations are used at a grid point. The lowest numbers are found in the western part of the tropical Pacific Ocean (about 120 observations). The number of day and night observations is about the same.

The ability of the objective method to produce gridded geophysical parameter fields with low rms error is investigated with ECMWF data interpolated onto satellite cells where individual satellite latent heat fluxes have been estimated (hereafter SimuEcmwf). The weekly latent heat flux fields, calculated from SimuEcmwf with the objective method, are compared to the weekly mean latent heat flux computed from 6-hourly ECMWF analyses. The global bias between the two weekly gridded Q_E fields does not exceed 2 W m^{-2} for all 17 weeks studied. The standard deviation of the difference is about 7 W m^{-2}. An example of the comparison between the weekly gridded SimuEcmwf and an ECMWF latent heat flux field is shown in Fig. 5. It presents the behavior of the differences for the period 6–12 January 1997 as a function of longitude, at five latitudes. The largest discrepancies are observed in regions of high variability of Q_E (Fig. 5e at 45°S, between 30° and 60°E) and/or near land (Figs. 5a and 5c in the vicinity of 50° and 105°E, respectively). Near land, SimuEcmwf samples are discarded due to the land effects a satellite sensor would have experienced.

TABLE 2. Statistical parameters characterizing the comparisons between weekly satellite-derived products and weekly averaged in situ (buoy and ships) and atmospheric analyses. The satellite and buoy statistics are computed for all weekly estimates during the study period (Oct 1996–Jun 1997). The satellite–ECMWF and satellite–NCEP–NCAR comparisons are limited to the 17 weeks defined in Table 1.

	Surface wind speed (m s^{-1})			Latent heat flux (W m^{-2})		
Data source	Mean (m s^{-1})	Std dev (m s^{-1})	Correlation	Mean (W m^{-2})	Std dev (W m^{-2})	Correlation
Satellite–buoy comparisons:						
Satellite	6.38	2.01		130	38	
TAO	5.90	2.34		126	29	
Satellite–TAO	0.62	1.52	0.88	4	26	0.79
Satellite	9.27	4.22		69	38	
ODAS	8.34	3.87		57	24	
Satellite–ODAS	0.66	2.33	0.83	12	21	0.88
Satellite	7.41	3.27		—	—	
NDBC	7.30	2.92		—	—	
Satellite–NDBC	0.11	1.70	0.91	—	—	—
Satellite–ship comparisons:						
Satellite	8.30	2.34		107	61	
Ship	8.97	2.83		96	63	
Satellite–ship	−0.53	1.64	0.81	−9	44	0.79
Satellite–ECMWF comparisons:						
Satellite	7.89	2.48		91	54	
ECMWF	7.41	2.47		113	69	
Satellite–ECMWF	0.48	0.91	0.93	−22	34	0.87
Satellite–NCEP–NCAR comparisons:						
Satellite	7.89	2.49		91	55	
NCEP–NCAR	7.31	2.56		99	64	
Satellite–NCEP–NCAR	0.58	1.07	0.91	−8	35	0.84

3. Comparison of weekly estimates

The weekly satellite-derived wind speeds and latent heat fluxes are compared with weekly averaged buoy and ship observations, and atmospheric analysis fields. Table 2 provides some statistical parameters characterizing the comparisons. The satellite and buoy statistics are computed for all weekly estimates during the study period (October 1996–June 1997), whereas correlation and difference statistics are estimated for all collocated data pairs.

a. Satellite–buoy comparisons

As stated in section 2a, 10-m neutral stratification buoy wind speeds are calculated from buoy wind speeds using the LKB model. The buoy specific air humidities are estimated from the buoy specific saturation humidity [using Eq. (6) and buoy SST] and relative humidity (or dewpoint). The bulk transfer coefficient is calculated from Eq. (3) using buoy neutral U_{10}. Therefore, buoy measurements allow the estimation of hourly buoy latent fluxes based on parameterization described by Eq. (2). For comparison purposes, the weekly averaged buoy data are calculated under the condition that for each week at least 72 hourly estimates are available.

For wind speed, Table 2 indicates that there is generally good agreement between buoy and satellite parameters. The main discrepancy is found for the ODAS wind speed comparison. This is related to the low number of collocated data, which is 125, and to the wind speed bias reported by P. Blouch, (2001, personal communication; see online at ftp://ftp.shom.fr/meteo/qc-stats) showing an underestimation of buoy winds with regard to numerical model estimates. The slopes of the linear regression between satellite/TAO, satellite/ODAS, and satellite/NDBC wind speeds are 1.19, 1.10, and 1.04, respectively. This means that the satellite fields tend to overestimate low wind speed and underestimate high wind speed. Even if such results are inherent in satellite wind speed evaluation (Freilich 1997) and mainly due to the fact that wind speed cannot be negative and, therefore, derived errors cannot be considered as a normal variable, comparison with TAO buoys needs further investigation. Indeed, the statistical parameters of the difference between satellite and TAO wind speeds are dependent on the buoy location. In the western part of the TAO network, satellite winds tend to be larger than those from buoys. In this region, the atmospheric liquid water content is high and can affect SSM/I and NSCAT wind retrievals (Halpern 1993; Wentz and Smith 1999). The discrepancy between the satellite and buoy winds can also be caused by degradation of the weekly averaged calculation due to the high wind variability (Bentamy et al. 1999). For buoys in the region 4°S–4°N, 160°E–90°W, the bias is mostly negative, implying an underestimation of satellite wind with respect to buoy estimates. The highest bias values are found in the eastern part of the network (2°S–2°N,

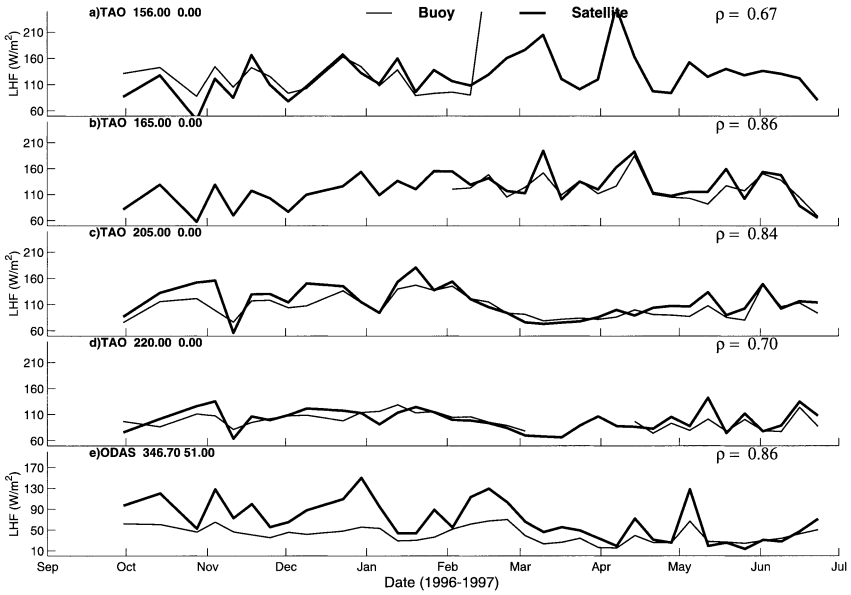

FIG. 6. Time series of weekly latent heat flux calculated from buoy hourly measurements (thin line) and from satellite data (solid line) at four TAO and one ODAS buoy locations.

120°–90°W), where they ranged between −0.45 and −1.5 m s^{-1} with a mean value of about −0.7 m s^{-1}. This may be due to the current, which is in the same direction as the winds (Quilfen et al. 2000). As mentioned in the data section and described by Bentamy et al. (2002), satellite winds used in this study are relative to the moving ocean surface. Therefore, satellite data can be underestimated compared to winds derived from moored buoys if the current or some substantial component of the current speed is parallel to the wind. The comparisons between satellite and NDBC data exhibit the best statistical results and show dependence on wind speed ranges or locations.

During the NSCAT period, satellite data and buoys exhibit similar statistical parameters of latent heat flux (Table 2). There are 1234 collocated data pairs of TAO and satellite latent heat fluxes, and 109 pairs of satellite/ODAS Q_E estimates. The latent heat flux derived from TAO measurements ranged between 45 and 390 W m^{-2}, with a mean value of 126 W m^{-2} and a standard deviation of 29 W m^{-2}. As expected, over the ODAS area the latent heat flux is lower than in the Tropics, with a mean value of 57 W m^{-2} and standard deviation of 24 W m^{-2}. These rms values for both TAO and ODAS comparisons are of the same order as those obtained by Schulz et al. (1997) in their comparison with in situ data. Figure 6 provides examples of satellite/buoy time series comparisons. The longest time series of weekly averaged buoy latent heat fluxes in the equatorial Pacific and ODAS regions are plotted.

The correlation coefficients, presented in Fig. 6, indicate good agreement between satellite and buoy Q_E estimates. Most weekly buoy Q_E variations are also exhibited by the satellite estimates. The correlation coefficients are high and significant at the 95% confidence level. The bias between satellites and ODAS buoys is significant (12 W m^{-2}). This is mainly due to the wind speed discrepancy. Indeed, between October 1996 and April 1997, ODAS buoys recorded lower winds than satellites. On average, the mean difference between satellite and ODAS buoy U_{10} estimates was about 1.35, reaching 2.1 m s^{-1} in February 1997. As indicated in section 2e, such a wind speed bias generates an error of about 10–20 W m^{-2} in latent heat flux estimation. Similar results were obtained when ODAS buoy winds were compared with ECMWF and ship winds. There is no dependency of Q_E error on buoy location for the ODAS network.

In comparisons of the surface wind estimates in the western part of the TAO region (5°S–5°N, 137°–165°E), the mean of the residual (satellite − TAO) was mainly positive and ranged between 1 and 25 W m^{-1}. In the eastern area (5°S–5°N, 110°–90°W), these values tend to be negative and vary between −2 and −32 W m^{-2}. Such bias behaviors are related to the overestimation and underestimation of satellite winds with respect to buoy winds in the western and eastern regions, respectively. In the middle of the tropical Pacific zone, the mean differences range between −2 and 17 W m^{-2}.

b. Satellite–ship comparisons

More than 2500 2° × 2° weekly averaged data are collocated between satellite and COADS during the period October 1996–June 1997: 80% are located in the North Atlantic and 20% in the eastern tropical Pacific. The two areas correspond to a wide range of latitudes and surface parameters. Wind speed ranges between 2

and 22 m s^{-1}. Table 2 indicates that the bias and the standard deviation of difference between satellite and ship wind speeds are -0.53 and 1.64 m s^{-1}, respectively. The estimate of a two-way orthogonal regression slope is 0.83, and the intercept is 0.96 m s^{-1}. Systematic shifts appear in low and especially in high wind speed ranges. For instance, for COADS winds higher than 12 m s^{-1} (13% of collocated data), the mean difference exceeds -2 m s^{-1} and the corresponding rms is greater than 2.5 m s^{-1}. For COADS wind speeds ranging between 2 and 12 m s^{-1}, the bias and rms differences are -0.35 and 1.50 m s^{-1}, respectively. Furthermore, there is no significant bias according to season or region. The main discrepancies between satellite and COADS wind speeds occur in areas where the number of ship observations used to calculate mean wind estimates over $2° \times 2°$ and 1 week is low (less than 30), so the error may be largely attributable to undersampling by the ships.

Ship latent heat fluxes are calculated from ship surface winds, specific surface and air humidity, SST, and air temperatures using the bulk formula in Eq. (2). Ship data are brought to neutral stability and the neutral bulk relations of Smith (1988) are used to calculate Q_E. The instantaneous ship Q_E is then weekly averaged over boxes of $2° \times 2°$. As shown in Table 2, the correspondence between satellite and ship latent heat flux estimates is good. The correlation coefficient of satellite and ship fluxes is about 0.80. It indicates that the physics of the latent heat flux is being accounted for in a coherent way. On average, the latent heat flux estimated from merged satellite data is lower than the ship latent heat flux, as one would expect from the wind speed comparisons. The investigation of the difference between satellite and ship Q_E as a function of season and region does not indicate any significant trend in terms of a linear regression analysis. For instance, the slope remains quite constant, varying between 0.96 and 1.06. However, the rms difference value is high at 44 W m^{-2}. As with the wind speed comparisons, such high scatter between satellite and ship is due to regions of low ship sampling. Excluding data pairs where the number of ship observations used to calculate weekly averaged latent heat flux is less than 30 improves the rms difference to 34 W m^{-2}.

c. Satellite–atmospheric model analyses

The weekly satellite surface wind speeds and latent heat fluxes are compared to ECMWF analysis and NCEP–NCAR reanalysis fields during the NSCAT period. The comparisons are performed over the global oceans between 60°S and 60°N for the 17 weeks listed in Table 1. More than 5×10^5 satellite–ECMWF and 1.5×10^5 satellite–NCEP–NCAR collocated data pairs are used in these comparisons, and the results are shown in Table 2.

The satellite wind speed estimates compare well with the wind speeds from the analyses. More than 99% of both ECMWF and NCEP–NCAR wind speeds used in the comparisons with the satellite data ranged between 1 and 16 m s^{-1}. The correlation coefficients are 0.93 for satellite–ECMWF and 0.91 for satellite–NCEP–NCAR. The mean wind speed difference is 0.48 m s^{-1} for satellite minus ECMWF and 0.58 m s^{-1} for satellite minus NCEP–NCAR. The differences are somewhat larger (smaller) for weaker (stronger) winds. For ECMWF and NCEP–NCAR wind speeds smaller than 7 m s^{-1}, the mean (satellite minus analysis) differences are 0.61 and 0.83 m s^{-1}, respectively. For ECMWF and NCEP–NCAR wind speeds greater than or equal to 7 m s^{-1}, the differences are 0.36 and 0.34 m s^{-1}, respectively.

The satellite latent heat flux estimates also show good general agreement with the latent heat fluxes from the analyses. The correlation coefficients for the latent heat flux comparisons give similar values to the wind speed comparisons: 0.87 for satellite–ECMWF and 0.84 for satellite–NCEP–NCAR. The mean latent heat flux differences are -22 W m^{-2} for satellite minus ECMWF and -8 W m^{-2} for satellite minus NCEP–NCAR. The mean difference is significantly larger for larger values of the fluxes. For ECMWF and NCEP–NCAR fluxes smaller than 100 W m^{-2} the mean (satellite minus analysis) differences are -6.5 and 3 W m^{-2}, respectively. For ECMWF and NCEP–NCAR latent heat fluxes greater than or equal to 100 W m^{-2} the differences are -35.8 and -21.9 W m^{-2}, respectively. By taking the ratio of the mean latent heat fluxes (analysis over satellite), we estimate that the ECMWF and NCEP–NCAR fluxes are about 25% and 9% larger than the satellite, respectively.

Figures 7 and 8 show examples of weekly averaged satellite fields of wind speed and latent heat flux for the week of 6–12 January 1997. Qualitatively, the corresponding ECMWF and NCEP–NCAR fields of wind speed and latent heat flux for that week look very similar to Figs. 7a and 8a (not shown). Quantitatively, however, there are significant differences between the satellite and the analyses fields for both wind speed (Figs. 7b and 7c) and latent heat flux (Figs. 8b and 8c). The wind speed difference maps (Figs. 7b and 7c) are dominated by positive satellite-minus-analysis differences (red) consistent with the positive wind speed bias estimated with the overall statistics in Table 2. However, the wind speed differences are not uniform. The regions of larger wind speed differences are the Indian Ocean between the equator and 20°S, the western and central equatorial Pacific, and the Atlantic and Pacific Oceans north of about 40°N. Low-latitude regions of positive (red) latent heat flux differences (Figs. 8b and 8c) correspond well with regions of positive wind speed differences (Figs. 7b and 7c), suggesting that the origin of the flux differences in those regions is the bias in wind speed. The latent heat flux difference maps (Figs. 8b and 8c) show large negative differences (blue) over regions where the fluxes are large: the Kuroshio and Gulf Stream currents, the northern Indian Ocean, the eastern North Pacific,

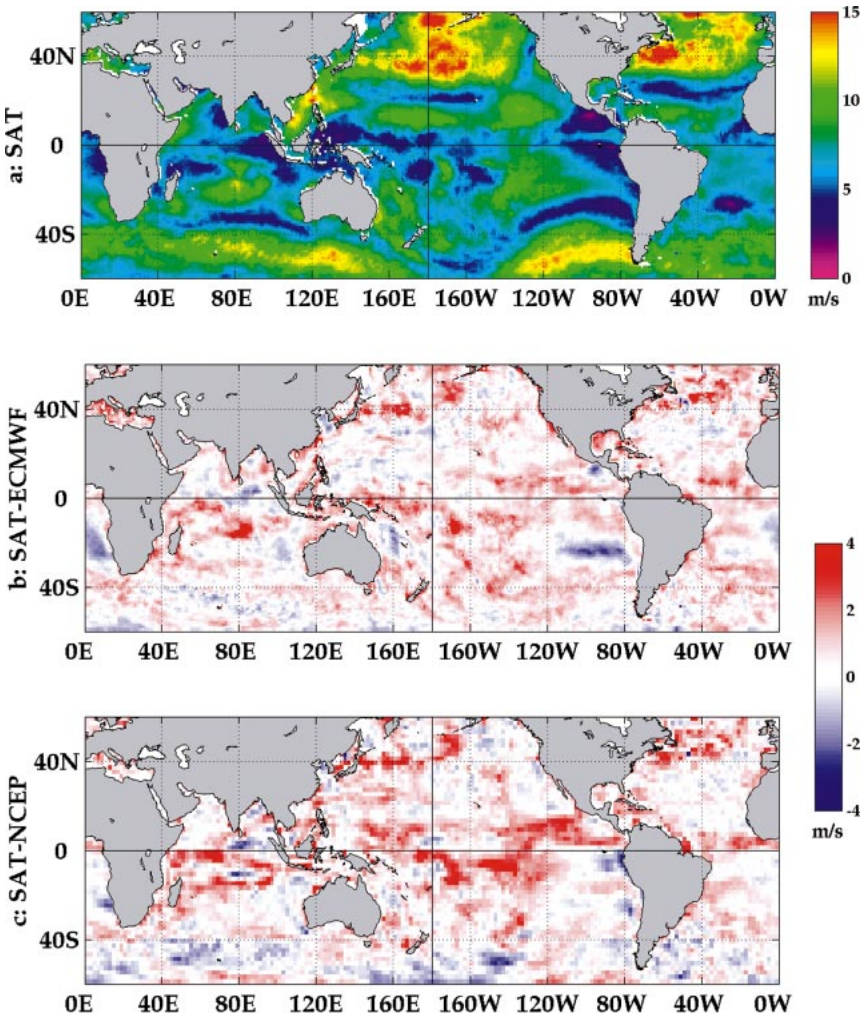

FIG. 7. (a) Map of weekly averaged satellite wind speed for the period 6–12 Jan 1997 and its difference with (b) ECMWF and (c) NCEP–NCAR weekly averaged wind speed fields for the same week.

and around Australia. In these regions, the flux differences cannot be explained by the wind speed bias.

4. Comparisons of monthly estimates

For further investigations, monthly averaged satellite surface wind speed and latent heat flux fields are compared to those derived from ECMWF and NCEP–NCAR in various 10° latitudinal bands and for different months. The aim of this study is to investigate the quality of satellite flux products and not to estimate the accuracy of numerical model flux estimates. The corresponding standard deviations and confidence intervals are also computed (not shown). Figure 9 shows examples of monthly averaged wind speeds as a function of longitude (0°–360°) for satellite (solid line), ECMWF (thin line), and NCEP–NCAR (dashed line) in three latitudinal bands and for two months: January 1997 and June 1997. The satellite and the analyses longitudinal series are quite similar for different latitudes and months. For most latitudes and months, the satellite–ECMWF and satellite–NCEP–NCAR longitudinal series are significantly correlated at the 95% level. They exhibit strong seasonal features at high latitudes. In the southern oceans, the highest wind speeds are found during April 1997 (not shown) in the Pacific Ocean and during June 1997 in the Indian Ocean. In the northern oceans, such winds occur during January 1997 in the middle part of the Pacific and in the western part of the Atlantic. In tropical regions, even though the dynamical range of surface winds is low compared to higher latitudes, a seasonal behavior is depicted. High winds occur during October 1996 (not shown) and January 1997, while low winds occur during April and June 1997. The satellite means tend to be larger than those of the analyses for all regions and months. Within the latitudinal band (40°–30°S), the weekly satellite wind speed shows some estimates of 20 m s^{-1}, which are not seen in the weekly

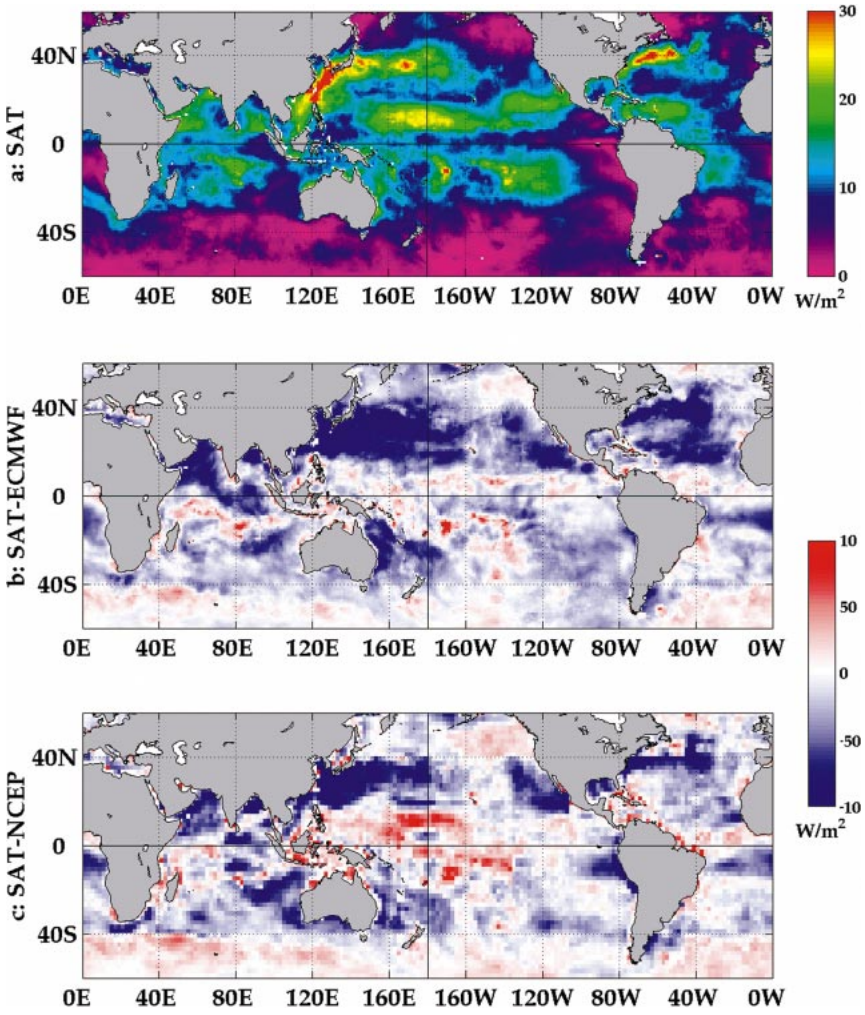

FIG. 8. (a) Map of weekly averaged satellite latent heat flux for the period 6–12 Jan 1997 and its difference with (b) ECMWF and (c) NCEP–NCAR weekly averaged latent heat flux fields for the same week.

averaged analyses. In the Tropics, a large bias (greater than 1.2 m s^{-1}) is found in the Pacific Ocean during June 1997. A fraction of this bias may be due to the satellite overestimation of low wind speeds.

Examining Table 2, along with Fig. 10, it is clear that the correspondence between the latent heat fluxes from satellite and atmospheric analyses is good. The latent heat flux estimates exhibit the main expected features. In general, the monthly averaged satellite estimates of Q_E exceeds 190 W m^{-2}, only between 40°S and 40°N. There are high values in the western part of the North Pacific and North Atlantic Oceans in January, due to the southward movement of the storms advecting cold, dry continental air over the sea (see also Fig. 8a). During the winter season, high latent heat fluxes are observed in the central Pacific and Atlantic, related to the return branch of the Hadley circulation. In the Indian Ocean, the highest values are found during June 1997, in conjunction with the monsoon event. In the tropical oceans, two maxima are depicted in the fall and winter seasons of the Northern Hemisphere. The first one is located in the warm pool region, and found to move eastward between October and January. This maximum seems to have a twin on the opposite side of the equator, northeast of Australia during June. The second maximum is located in the central Pacific with an eastward shift between January and June. The lowest tropical values are in the equatorial cold tongue and are more pronounced in the Pacific Ocean than in the Atlantic Ocean. Very low latent heat flux values are found in high northern latitudes in June, which are, of course, related to the frequency of fog in these areas during summer when warm air flows northward over cold water.

The comparison between satellite data and atmospheric analyses reveals a strong seasonal difference in magnitude during the fall and winter months in both the northern and southern oceans. For instance, within the latitudinal band 30°–40°N, and within the Kuroshio and

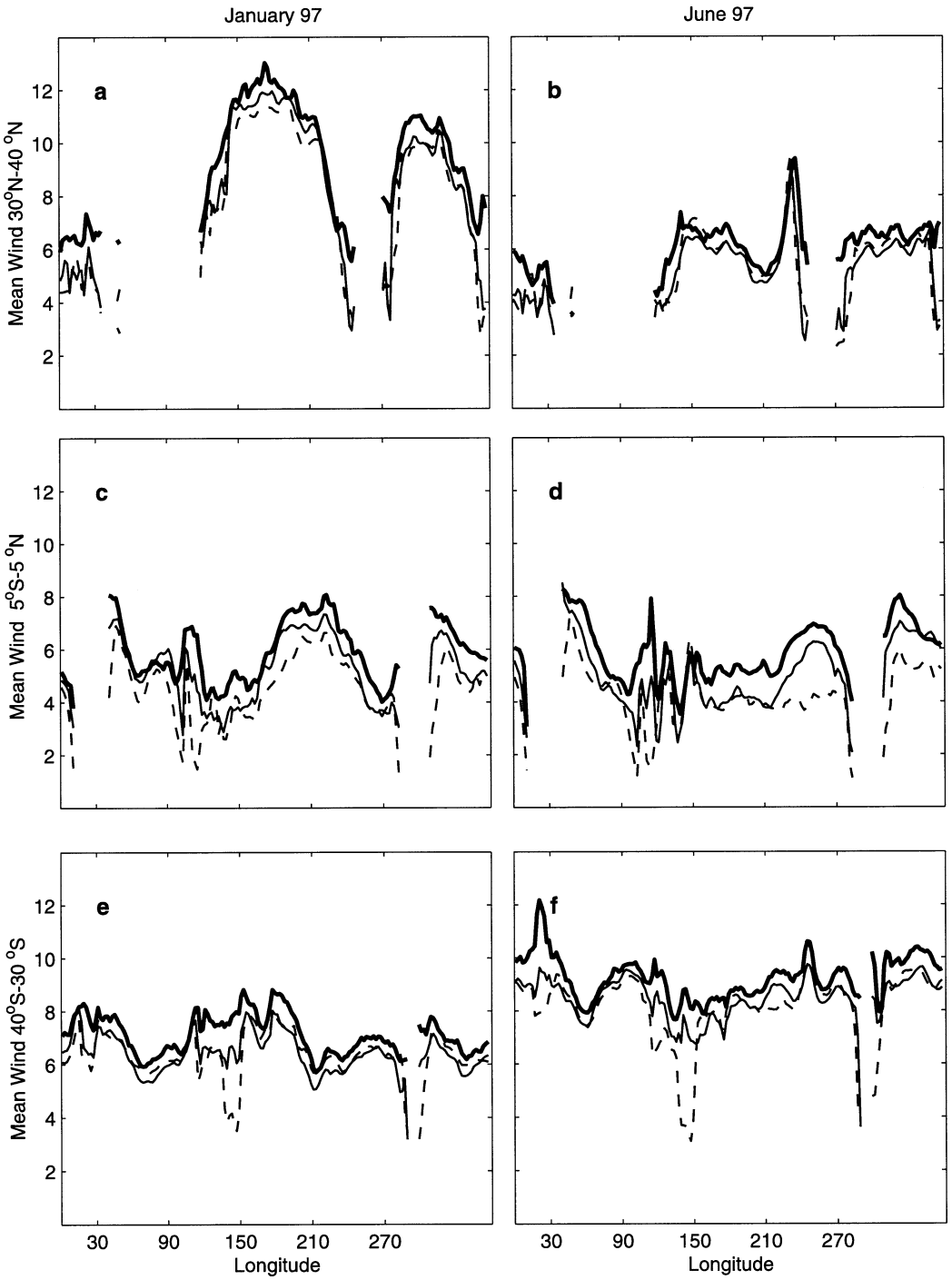

FIG. 9. Monthly wind speed averages as a function of longitude (0°–360°) for satellite (solid line), ECMWF (thin line), and NCEP–NCAR (dashed line) in three latitudinal bands for Jan and Jun 1997.

Gulf Stream regions, the high latent heat fluxes during January 1997 lead, in turn, to large negative biases between the satellite and the analyses. This is not consistent with the wind comparisons (Fig. 9), which, in these areas, show that satellites provide slightly higher winds than the analyses (maximum mean difference does not exceed 0.90 m s^{-1}). The maximum monthly Q_E difference during January 1997 within the longitudinal bands of 123°–157°E and 57°–90°W (Fig. 10a) is about 70 W m^{-2}. This is about twice the global mean rms difference during the NSCAT period (Table 2). The maximum values of latent heat flux standard deviation are also found

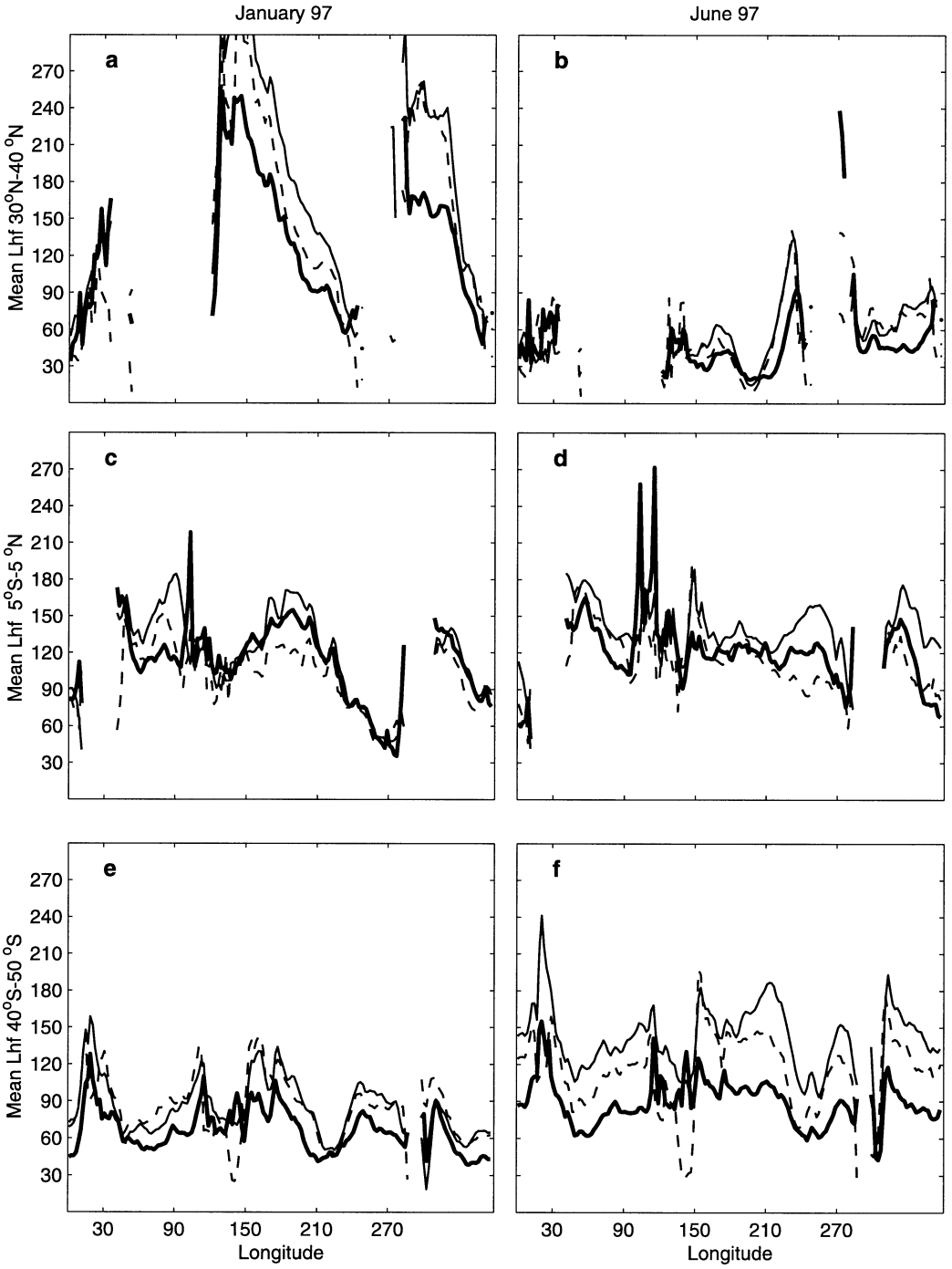

FIG. 10. Same as Fig. 9, except for monthly averaged latent heat flux.

in these regions and during these seasons. The errors in the satellite estimates are likely to be large here due to our inability to account for cold air outbreaks and associated stratification effects on the fluxes. The confidence intervals corresponding to the analyses mean values are also large. For instance, in the western part of the Pacific and Atlantic Oceans where the mean differences are high, the ECMWF 95% confidence intervals are about (20, 490) and (70, 470) W m^{-2}, respectively.

Further investigations of the mean differences are made using ship surface fluxes as a third data source. All validated weekly satellite, ECMWF, and ship data (U, SST, q_a, q_s, Q_E) available over the region limited by 90°–30°W in longitude and 30°–40°N in latitude, are

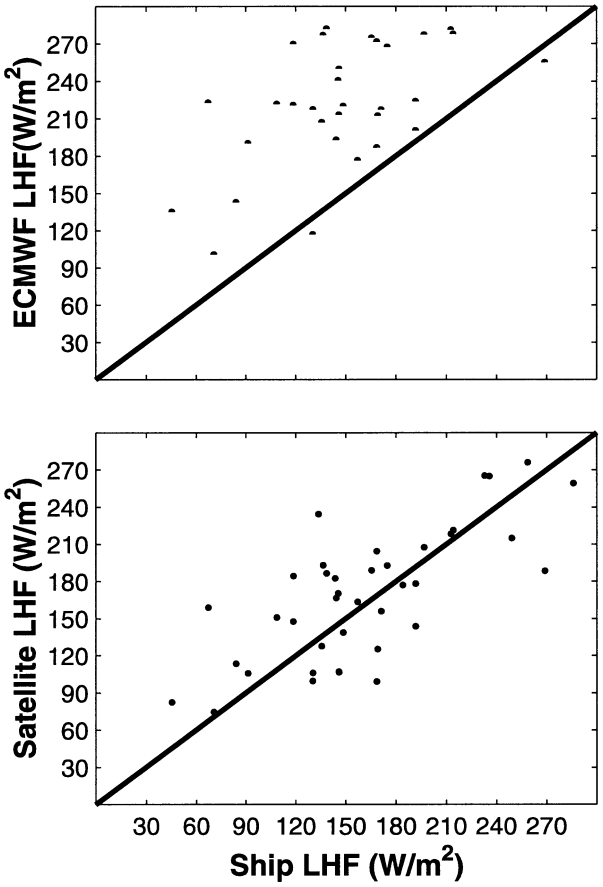

FIG. 11. Comparison between three weekly averaged latent heat flux estimates: from ship, ECMWF, and satellite data over the western North Atlantic within the longitudinal band 30° and 60°W, and latitudinal band 30° and 40°N, during Jan 1997.

spatially collocated. The sample size of the collocated triplet dataset is 24 during January 1997. Figure 11 shows the comparison between the three latent heat flux estimates. Compared to the ship data, satellite latent heat fluxes are overestimated by 7 W m^{-2}, while ECMWF fluxes are overestimated by 73 W m^{-2}. Hence, we attribute the difference between satellite and ECMWF Q_E estimates to be due to an overestimation by the ECMWF model.

The main source of error between satellite and ECMWF comes from the difference in the specific air humidity. Indeed, q_a values derived from ECMWF analyses are lower than satellite q_a values. For the region of high Q_E discrepancy, the mean difference between satellite and ECMWF q_a estimates is about 1.8 g kg^{-1}. As expected, the difference between satellite and ship is low. For a SST of about 16°C and a wind speed of about 11 m s^{-1}, the bias in latent heat flux due to a bias in q_a of 1.8 g kg^{-1} is of the order of 50 W m^{-2} (see section 2e). Further investigations indicate that the difference between satellite and ECMWF may be related to wind direction distribution. In the region of high discrepancy between ECMWF and satellite Q_E during January 1997, the winds are frequently northerly (about half of the time). The air temperature derived from ECMWF analysis is on average 2° colder than ship data, producing lower specific air humidity values and, in turn, higher latent heat flux estimates. We, therefore, suggest that ECMWF Q_E estimates are probably too high in these conditions.

An additional source of error is related to the exchange coefficients. During January and within the high discrepancy region, the surface wind speed varies between 9 and 13 m s^{-1}, with mean values of about 11 m s^{-1} for satellite and 10.4 m s^{-1} for ECMWF. Within this wind speed range, the exchange coefficient C_E estimated from Eq. (4) is quite constant at 1.10×10^{-3}. For ECMWF latent heat flux analysis (Beljaars and Viterbo 1998), C_E increases from 1.10×10^{-3} to 1.15×10^{-3}. Therefore, the difference between the exchange coefficients used for satellite and for ECMWF latent heat flux estimates can explain more than 10 W m^{-2} of the difference between the satellite and ECMWF (section 2e).

We point out that our finding agrees with the Josey (2001) results. He established that the latent heat fluxes estimated from European buoy data are lower than ECMWF analysis and NCEP–NCAR reanalysis estimates. This agrees with the results of Zeng et al. (1998), which showed that the numerical schemes have higher exchange coefficients compared to values derived from the TOGA COARE experiment (Fairall et al. 1996).

5. Summary and discussion

This paper presents weekly and monthly averaged fields of surface wind and latent heat flux on a global $1° \times 1°$ grid. They have been calculated from radar and radiometer estimates of surface variables for the period October 1996–June 1997. The results are encouraging, showing generally good agreement and consistency with buoy and ship data and with winds and latent heat fluxes from atmospheric analyses, but with enough differences with the latter that the satellite estimates will serve to test the adequacy of the analyses.

We use merged data from *ERS-2* and NSCAT scatterometers, and from four of the SSM/I radiometers. A simulation experiment showed that the frequent sampling realizes minimal aliasing effects at the scales of interest even for areas of high surface parameter variability, where poor sampling by one polar-orbiting satellite will not suffice. The merging procedure and the objective method used in this paper both provide an effective approach for calculating daily, weekly, and monthly fields with accuracy of interest to climate studies. Such accuracy has been estimated through comparisons with buoy and ship data and by comparison to ECMWF and NCEP analyses.

For wind speed, the agreement between satellite data and buoys is good, except for the ODAS network. The

rms difference values are less than 1.7 m s^{-1} for NDBC and TAO buoy comparisons, while for ODAS the rms is 2.3 m s^{-1}. The difference between satellite and ODAS winds is significantly larger during the period October–December 1996 than during the rest of the study period. No such difference behavior was found for the NDBC and TAO buoys. The cause of the underestimation of ODAS buoy winds between October and December 1996 with respect to satellite estimates is unknown. Satellite wind speeds exhibit positive bias versus TAO and ODAS wind estimates. Excluding periods of known errors, the satellite wind bias drops to a value of about 0.2 m s^{-1}. The comparison with NDBC wind data provided a small positive bias. Similar results have been found for weekly averaged satellite and COADS wind speed comparisons. However, the satellite wind speeds are biased about 0.5 m s^{-1} low with respect to COADS ship winds. This may be related to some uncertainty in values for ship anemometer heights. At global scales, the representativeness of satellite winds were evaluated through comparisons with ECMWF and NCEP–NCAR wind analyses. The main results are that the correlation between satellite and analyses winds is high (greater than 0.9), the rms differences are about 1 m s^{-1}, and the model wind speeds are between 0.1 and 0.9 m s^{-1} lower than satellite estimates. Through these various wind speed comparisons, it was found that the highest error values (rms values exceeding 1.80 m s^{-1}) correspond to areas with strong surface currents, such as the western part of the tropical Pacific and/or areas near coasts or islands and in regions where satellite sampling is poor.

In this paper, the estimation of latent heat flux from radar and radiometer measurements was mainly based on the Schulz et al. (1993, 1997) approach. However, the specific air humidity retrieved from SSM/I brightness temperatures via the Schulz model revealed a seasonal bias versus ship Q_E estimates. To remove this bias, a new model relating SSM/I brightness temperatures and q_a was established and used for latent heat flux calculation through a bulk formula.

The agreement between satellite and in situ data is good enough to suggest that these Q_E sources are achieving their accuracy goals. It was shown that the satellite weekly Q_E exhibited the main known spatial and temporal characteristics at global as well as at local scales. For instance, the local variability of Q_E is well revealed by the satellite time series in tropical and in North Atlantic areas (with respect to TAO, ODAS buoy, and ship data).

The comparisons between weekly latent heat flux values estimated from merged satellite observations and from buoys provided a root-mean-square error less than 30 W m^{-2}. For ship comparisons, the rms is somewhat larger. Excluding the errors due to the sampling period of ship observations, the rms drops to 34 W m^{-2}. We compared the satellite derived latent heat fluxes over the global oceans with ECMWF analyses and NCEP–NCAR reanalyses. High correlations between satellite and model Q_E were found. However, it appears that the ECMWF and NCEP–NCAR analyses overestimate the latent heat flux by about 20% and 10%, respectively, with regard to satellite values. This is mainly due to the uncertainty in relating surface layer fields of the model to surface fluxes using a bulk formula. Beljaars (1994) and Zeng et al. (1998) suggest that ECMWF and NCEP–NCAR use C_E values that are too high. In this paper, the bulk algorithm used a latent heat exchange coefficient based on Smith (1988) and Hasse and Smith (1997). The bulk algorithm used in the ECMWF model is by Beljaars (1994). When calculating ECMWF latent heat flux using the same bulk formulas as we used for the satellite estimates (2), the mean value of satellite-minus-ECMWF latent heat flux estimates is about 7 W m^{-2}. The remaining bias is related to the higher values of satellite surface winds with respect to ECMWF wind analysis, which is probably due to the difference in the effective scales between the numerical model and the satellite observations.

Our estimates of wind fields and latent heat flux fields described here rely only on satellite data. If wind stress (momentum flux) is sought, then the neutral 10-m equivalent wind provided by the scatterometer and radiometer calibrations is the correct input to a bulk formula employing a neutral drag coefficient. Similarly, for latent heat flux when using the 10-m neutral value of C_E, the neutral 10-m equivalent wind speed estimate is appropriate. Our method inserts an error in that we do not correct our estimated q_a to neutral stratification, since that would require input for T_a at 10 m or $(T_s - T_a)$, for which no satellite method has yet been established. The approximation that $q_s - q_a$ calculated from SST and SSM/I brightness temperatures represents the neutral equivalent humidity difference is good for high wind speed conditions as found in the Southern Ocean year-round. It may introduce some regional biases in low wind conditions, such as where the air–sea temperature differences and atmospheric stratification values are large (positive or negative). However, we do not expect the total error to be large, since the winds are neutral equivalent and most of the ocean is in near-neutral stratification most of the time and especially with regards to the averaging period. This was verified by comparing COADS q_a in various regions and seasons with and without stability corrections. The difference in q_a due to the stability correction is on the order of 1%. Future work should explore ways of including the stratification correction. Methods for doing that include using a Bowen ratio estimate, which can be taken from one of the numerical analyses, or from information on atmospheric structure provided by satellite (Konda et al. 1996), possibly the TIROS Operational Vertical Sounder (TOVS). If a numerical model analysis is part of the evaluation of the flux, we suggest a hybrid method that assimilates the satellite information into the surface layer fields from the model (with minimal loss of the measured data,

even if full adjustment of the model is sacrificed). If the merged satellite and model fields can be made to fully reflect the observed values, the new fields could provide a superior means to more adequately interpolate in time and space, including short-term advection of storms and frontal boundaries and better inclusion of local stratification variations.

This study of the accuracy of surface winds and latent heat fluxes calculated from merged radar and radiometer surface variables allows the calculation of long time series of gridded fields that will facilitate the systematic study of the temporal and spatial variability of flux variables over the global oceans. Keeping in mind the inherent uncertainties in bulk formula parameterization, the accuracy of the resulting satellite flux fields is within the bounds of the observational errors. Therefore, such fields will allow computation of the main surface flux characteristics (spectra, correlation matrices, structure functions) without the need for further smoothing. Furthermore, they will be used to force an ocean circulation model like that developed by Laboratoire Oceanographique Dynamique et de Climatologie (LODYC; Madec et al. 1998) to evaluate the impact of satellite input versus in situ measurements retrieved from some dedicated oceanic experiments. Production of a full decade (1991–2001) of these flux fields (including stress, divergence, and curl from the wind field) has been planned. Such calculations will also be performed with retrieved wind vectors from SeaWinds on *QuikSCAT* and *ADEOS-2*.

Acknowledgments. This research was supported by NASA Grant UPN261-75 to AOML and by the Institut Français pour la Recherche et l'Exploitation de la Mer (IFREMER). We gratefully acknowledge J. Harris for help with the reanalysis fields and G. Derr for assistance with document production. We are grateful to the CERSAT team for making available the validated and calibrated ERS, NSCAT, and SSM/I data. We also acknowledge Drs. H. Graber and Y. Quilfen for their help and support.

REFERENCES

Ataktürk, S. S., and K. B. Katsaros, 1998: Estimates of surface humidity and wind speed obtained from satellite data in the stratocumulus regime in the Azores region. *Remote Sensing of the Pacific Ocean by Satellites,* R. A. Brown, Ed., Southwood Press, 16–22.

Baumgartner, A., and E. Reichel, 1975: *The World Water Balance.* Elsevier Science, 179 pp.

Beljaars, A. C. M., 1994: The impact of some aspects of the boundary layer scheme in the ECMWF model. *Proc. Seminar on Parameterization of Sub-Grid Scale Processes,* Reading, United Kingdom, European Centre for Medium-Range Weather Forecasts, 125–161.

——, and P. Viterbo, 1998: The role of the boundary layer in a numerical weather prediction model. *Clear and Cloudy Boundary Layers,* A. A. M. Holtslag and P. G. Dunkerke, Eds., Royal Netherlands Academy of Arts and Science, 287–304.

Bentamy, A., Y. Quilfen, P. Quefeulou, and A. Cavanié, 1994: Calibration and validation of the ERS-1 scatterometer. IFREMER Tech. Rep. DRO/OS-94-01, 80 pp.

——, ——, F. Gohin, N. Grima, M. Lenaour, and J. Servain, 1996: Determination and validation of average field from ERS-1 scatterometer measurements. *Global Atmos.–Ocean Syst.,* **4,** 1–29.

——, P. Queffeulou, Y. Quilfen, and K. Katsaros, 1999: Ocean surface wind fields estimated from satellite active and passive microwave instruments. *IEEE Trans. Geosci. Remote Sens.,* **37,** 2469–2486.

——, K. B. Katsaros, W. M. Drennan, and E. B. Forde, 2002: Daily surface wind fields produced by merged satellite data. *Gas Transfer at Water Surfaces, Geophys. Monogr.,* No. 127, Amer. Geophys. Union, 343–349.

Bunker, A. F., 1976: Computations of surface energy flux and annual air–sea interaction cycles of the North Atlantic Ocean. *Mon. Wea. Rev.,* **104,** 1122–1140.

Courtier, P., and Coauthors, 1998: The ECMWF implementation of three-dimensional variational assimilation (3D-Var). I: Formulation. *Quart. J. Roy. Meteor. Soc.,* **124B,** 1783–1807.

da Silva, A. M., C. C. Young, and S. Levitus, 1994: *Anomalies of Fresh Water Fluxes.* Vol. 4, *Atlas of Surface Marine Data,* NOAA Atlas NESDIS 9, 308 pp.

——, ——, and ——, 1995: Towards a revised Beaufort equivalent scale. *Proc. Int. COADS Winds Workshop,* Kiel, Germany, National Oceanic and Atmospheric Administration, 270–286.

DeCosmo, J., K. B. Katsaros, S. D. Smith, R. J. Anderson, W. Oost, K. Bumke, and H. Chadwick, 1996: Air–sea exchange of water vapor and sensible heat: The Humidity Exchange Over the Sea (HEXOS) results. *J. Geophys. Res.,* **101,** 12 001–12 016.

Esbensen, S. K., and Y. Kushnir, 1981: The heat budget of the global ocean: An atlas based on estimates from surface marine observations. Climatic Research Institute, Oregon State University Rep. 29, 27 pp. and 188 figs.

——, D. B. Chelton, D. Vickers, and J. Sun, 1993: An analysis of errors in Special Sensor Microwave/Imager evaporation estimates over the global oceans. *J. Geophys. Res.,* **98,** 7081–7101.

Fairall, C. W., E. F. Bradley, D. P. Rogers, J. B. Edson, and G. S. Young, 1996: Bulk parameterization of air–sea fluxes for TOGA-COARE. *J. Geophys. Res.,* **101,** 3747–3764.

Freilich, M. H., 1997: Validation of vector magnitude datasets: Effect of random component errors. *J. Atmos. Oceanic Technol.,* **14,** 695–703.

Gleckler, P. J., and B. C. Weare, 1997: Uncertainties in global ocean surface heat flux climatologies derived from ship observations. *J. Climate,* **10,** 2764–2781.

Goldenberg, S. B., C. W. Landsea, A. M. Mestas-Nuñez, and W. M. Gray, 2001: The recent increase in Atlantic hurricane activity: Causes and implications. *Science,* **293,** 474–479.

Goodberlet, M. A., C. T. Swift, and J. C. Wilkerson, 1989: Remote sensing of ocean surface winds with the Special Sensor Microwave/Imager. *J. Geophys. Res.,* **94,** 14 547–14 555.

Grima, N., A. Bentamy, K. Katsaros, and Y. Quilfen, 1999: Sensitivity of an oceanic general circulation model forced by satellite wind stress fields. *J. Geophys. Res.,* **104,** 7967–7989.

Halpern, D., 1993: Validation of Special Sensor Microwave/Imager monthly mean wind speeds from July 1987 to December 1989. *IEEE Trans. Geosci. Remote Sens.,* **31,** 692–699.

——, V. Zlotnicki, P. Woiceshyn, O. Brown, M. Freilich, and F. Wentz, 1998: An atlas of monthly mean distributions of SSM/I surface wind speed, AVHRR sea surface temperature, AMI surface wind velocity, and TOPEX/POSEIDON sea surface height during 1996. Jet Propulsion Laboratory, Publ. 98-11, 101 pp.

Hasse, L., and S. D. Smith, 1997: Local sea surface wind, wind stress, and sensible and latent heat fluxes. *J. Climate,* **10,** 2711–2724.

Isemer, H. J., and L. Hasse, 1987: *The Bunker Climate Atlas of the North Atlantic Ocean.* Vol. 2. Springer-Verlag, 252 pp.

Jet Propulsion Laboratory, 1996: NASA scatterometer science data product users manual: Overview and geophysical data products. Jet Propulsion Laboratory, Publ. D-12985, 66 pp.

Josey, S. A., 2001: A comparison of ECMWF, NCEP–NCAR, and SOC surface heat fluxes with moored buoy measurements in the

subduction region of the northeast Atlantic. *J. Climate,* **14,** 1780–1789.

Jourdan, D., P. Peterson, and C. Gauthier, 1997: Oceanic freshwater budget and transport as derived from satellite radiometric data. *J. Phys. Oceanogr.,* **27,** 457–467.

Kalnay, E., and Coauthors, 1996: The NCEP/NCAR 40-Year Reanalysis Project. *Bull. Amer. Meteor. Soc.,* **77,** 437–472.

Kent, E. C., and P. K. Taylor, 1995: A comparison of sensible and latent heat flux estimates for the North Atlantic Ocean. *J. Phys. Oceanogr.,* **25,** 1530–1549.

Konda, M., N. Imasato, and A. Shibata, 1996: A new method to determine near sea surface air temperature by using satellite data. *J. Geophys. Res.,* **101,** 14 349–14 360.

Landsea, C. W., R. A. Pielke, A. M. Mestas-Nuñez, and J. A. Knaff, 1999: Atlantic basin hurricanes: Indices of climatic changes. *Climatic Change,* **42,** 89–129.

Lindau, R., 1995: A new Beaufort equivalent scale. *Proc. Int. COADS Winds Workshop,* Kiel, Germany, National Oceanic and Atmospheric Administration, 232–252.

Liu, W. T., 1986: Statistical relation between monthly precipitable water and surface-level humidity over global oceans. *Mon. Wea. Rev.,* **114,** 1591–1602.

——, K. B. Katsaros, and J. A. Businger, 1979: Bulk parameterization of air–sea exchanges of heat and water vapor including the molecular constraints at the interface. *J. Atmos. Sci.,* **36,** 1722–1735.

Louis, J.-F., 1979: A parametric model of vertical eddy fluxes in the atmosphere. *Bound.-Layer Meteor.,* **17,** 187–202.

Madec, G., P. Delecluse, M. Imbard, and C. Lévy, 1998: OPA 8.1 ocean general circulation model reference manual. Note du Pole de Modelisation, Institut Pierre-Simon Laplace, Paris, France, N11, 91 pp.

Maroni, C., 1996: Offline wind field production. *CERSAT News,* No. 5, IFREMER Publ., 2–3. [Available online at http://www.ifremer.fr/cersat/FICHES/CNEWS/E_CNEWS.htm.]

Miller, D. K., and K. B. Katsaros, 1992: Satellite derived surface latent heat fluxes in a rapidly intensifying marine cyclone. *Mon. Wea. Rev.,* **120,** 1093–1107.

Petty, G. W., and K. B. Katsaros, 1992: *Morning–Evening Differences in Global and Regional Oceanic Precipitation as Observed by the SSM/I.* Purdue University Press, 4 pp.

——, and ——, 1994: The response of the SSM/I to the marine environment. Part II: A parameterization of the effect of the sea surface slope distribution on emission and reflection. *J. Atmos. Oceanic Technol.,* **11,** 617–628.

Quilfen, Y., 1995: *ERS-1* off-line wind scatterometer products. IFREMER Tech. Report, 75 pp.

——, A. Bentamy, P. Delecluse, K. B. Katsaros, and N. Grima, 2000: Prediction of sea level anomalies using ocean circulation model forced by scatterometer wind and validation using TOPEX/Poseidon data. *IEEE Trans. Geosci. Remote Sens.,* **38,** 1871–1884.

Reynolds, R. W., and T. M. Smith, 1994: Improved global sea surface temperature analyses using optimum interpolation. *J. Climate,* **7,** 929–948.

Schlüssel, P., L. Schanz, and G. English, 1995: Retrieval of latent heat flux and long wave irradiance at the sea surface from SSM/I and AVHRR measurements. *Adv. Space Res.,* **16,** 107–115.

Schmitt, R. W., and S. E. Wijffels, 1993: The role of the ocean in the global water cycle. *Interactions between Global Climate Subsystems, Geophys. Monogr.,* No. 75, Amer. Geophys. Union, 77–84.

Schulz, J., P. Schlüssel, and H. Grassl, 1993: Water vapor in the atmospheric boundary layer over oceans from SSM/I measurements. *Int. J. Remote Sens.,* **14,** 2773–2789.

——, J. Meywerk, S. Ewald, and P. Schlüssel, 1997: Evaluation of satellite-derived latent heat fluxes. *J. Climate,* **10,** 2782–2795.

Smith, S. D., 1988: Coefficients for sea surface wind stress, heat flux and wind profiles as a function of wind speed and temperature. *J. Geophys. Res.,* **93,** 15 467–15 472.

Soden, B. J., 1999: How well can we monitor and predict an intensification of the hydrological cycle? *GEWEX News,* Vol. 9, No. 3, 4–5.

Taylor, P. K., E. C. Kent, M. J. Yelland, and B. I. Moat, 1995: The accuracy of wind observations from ships. *Proc. Int. COADS Winds Workshop,* Kiel, Germany, National Oceanic and Atmospheric Administration, 132–155.

Wentz, F. J., and D. K. Smith, 1999: A model function for the ocean-normalized radar cross-section at 14 GHz derived from NSCAT observations. *J. Geophys. Res.,* **104,** 11 449–11 514.

——, L. A. Mattox, and S. Peteherych, 1986: New algorithms for microwave measurements of ocean winds: Applications to Seasat and the Special Sensor Microwave/Imager. *J. Geophys. Res.,* **91,** 2289–2307.

Woodruff, S. D., H. F. Diaz, J. D. Elms, and S. J. Worley, 1998: COADS release 2 data and metadata enhancements for improvements of marine surface flux fields. *Phys. Chem. Earth,* **23,** 517–526.

Zeng, X., M. Zhao, and R. E. Dickinson, 1998: Intercomparison of bulk aerodynamic algorithms for the computation of sea surface fluxes using TOGA-COARE and TAO data. *J. Climate,* **11,** 2628–2644.